UNIVERSIDADE DE SÃO PAULO

INSTITUTO DE FÍSICA
CAIXA POSTAL 66318
05389-970 SÃO PAULO - SP
BRASIL

PUBLICAÇÕES

IFUSP/P-1238

A SYMPLETIC MAPPING FOR THE ERGODIC MAGNETIC LIMITER AND ITS DYNAMICAL ANALISYS

K. Ullmann; I.L. Caldas
Instituto de Física, Universidade de São Paulo

Setembro/199

A SYMPLETIC MAPPING FOR THE ERGODIC MAGNETIC LIMITER AND ITS DYNAMICAL ANALISYS

K. Ullmann†, I.L. Caldas‡

Instituto de Física da Universidade de São Paulo
C.P. 66318, 05389-970 São Paulo, Brazil

Abstract - A model for a new bidimensional sympletic mapping describing the field line trajectories in a tokamak perturbed by ergodic magnetic limiter coils is presented. Numerical examples of the field line trajectories with toroidal correction of the equilibrium are computed. Also the importance of the sympleticity of the new mapping regarding certain features of nonlinear dynamical analisys is shown, and some standard algorithms, such as the computation of Lyapunov exponents and safety factors, are applied.

1 Introduction

Low-dimensional mappings [1, 2] were widely used in the last few years for studying the qualitative behaviour of new phenomena observed in more complex systems, such as nonlinear systems of differential equations. This led to a much better understanding of non-linear phenomena, such as strange attractors, sensibility to initial conditions and, specially, the several kinds of transitions from order to chaos, such as period-doubling, intermittency, torus-breakdown, etc... [3, 4].

But even if there are many results concerning some model maps [5, 6], such as, e.g., the logistic, the circle, the standard, and the Ulam map, there are still few works about maps which are more closely related to experimental systems of interest, describing at least their qualitative behaviour [7, 8]. One of the experimental phenomena which has been studied with the aid of maps is the ergodization of magnetic equilibrium field lines at the plasma edge,

when perturbed by the action of an ergodic magnetic limiter [9, 10, 11]. The concept of an ergodic magnetic limiter was introduced in the late seventies and is based on the idea that a chaotic boundary layer of field lines, which could act as a plasma limiter and so lower the impurity levels at the core, could appear as a result of resonant magnetic disturbing fields perturbing the equilibrium magnetic fields which contains the plasma. This magnetic ergodic limiter consists of a grid-shaped coil wound around the tokamak vessel and conducting a current, generating these disturbing fields.

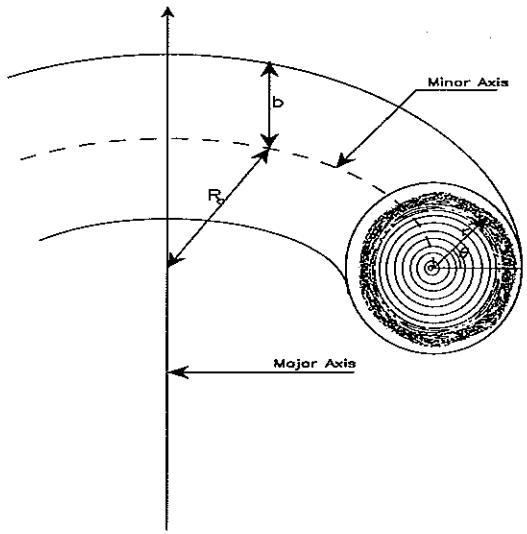

Figure 1: Essential geometry of the Tokamak.

This quite complex phenomenum can be well described by maps because the equation of the equilibrium field lines ($\vec{B} \times d\vec{l} = 0$) outside the influence region of the ergodic magnetic limiter can be analitically integrated, with some minor approximations, and so we deal with a quasi-integrable system, once we consider the influence region of the limiter coils narrow enough [8].

Considering the tokamak as a toroidal camera with major radius R_0 and minor radius b (fig.1) we will study the magnetic field line evolution analysing a Poincaré section which consists of a straight cut of the tokamak vessel at the center of the ergodic magnetic limiter. The point where the field line

cuts this Poincaré section will be given in polar coordinates (r,θ) with their origin located at the minor tokamak axis.

This paper is organized as follows : in the second section we study the previously existent models of the ergodic magnetic limiter. In section 3 we introduce our sympletic model for the mapping of the field line trajectories. Then we perform the dynamical analisys of the field lines generated by our model, computing Lyapunov exponents and rotational transforms [12, 13] in section 4. Section 5 is devoted to the analisys of the model with varying initial conditions and parameters. Our conclusions are presented in the last section.

2 The previous models

One of the first models describing the magnetic field line evolution in a tokamak camera perturbed by ergodic magnetic limiter coils is the Martin-Taylor mapping [14, 15, 16], which consists of two consecutive bidimensional mappings. The first mapping describes the evolution of the magnetic field line along the tokamak vessel (equilibrium field) and is given by:

$$x_n^* = x_n + s y_n \qquad (2.1.a)$$

$$y_n^* = y_n \qquad (2.1.b)$$

where (x_n, y_n) are the rectangular coordinates of the initial position of the field line in the Poincaré plot, (x_n^*, y_n^*) the rectangular coordinates of the final position, and $s = -\frac{2\pi b}{q^2}\frac{dq}{dy}$ is the strength of the shear of the equilibrium field (b is the minor tokamak radius and $q(y)$ the safety factor profile, which is related to the rotational transform ι by $q = \frac{2\pi}{\iota}$).

The second mapping describes the field line evolution in the region of the diffuser grid of 'wave length' $\frac{2\pi b}{m}$ with a current I in each wire of length l, and is given by:

$$x_{n+1} = x_n^* - p e^{-y_n^*} \cos x_n^* \qquad (2.2.a)$$

$$y_{n+1} = y_n^* + \ln(\cos(x_n^* - p e^{-y_n^*} \cos x_n^*)) - \ln(\cos x_n^*) \qquad (2.2.b)$$

where $p = \frac{\pi m^2 l I}{b^2 B_0}$ measures the strength of the diffuser relative to the toroidal field (B_0 is the intensity of the toroidal field, that is, the magnetic field component along the tokamak camera). In most cases where this mapping was

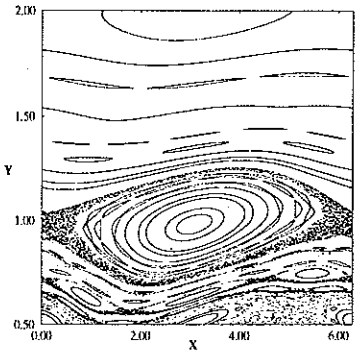

Figure 2: Martin-Taylor mapping with $p = 0.30$ and $s = 2\pi$

analyzed the magnetic shear $\frac{dq}{dy}$ was considered as being constant in the studied region, and in this case the mapping depends only on two dimensionless parameters p and s. It is also important to observe that, as both consecutive mappings have unitary Jacobians ($\frac{\partial(x_n^*, y_n^*)}{\partial(x_n, y_n)} = \frac{\partial(x_{n+1}, y_{n+1})}{\partial(x_n^*, y_n^*)} = 1$), the whole mapping is area-preserving, and can be described in a Hamiltonian formulation.

Using this mapping to plot a Poincaré section with constant parameters p and s (fig.2), we observe the typical island chain structure with chaotic regions around the destroyed separatrixes and secondary island chains around the main islands[17, 18]. Although this model describes very well the qualitative behaviour of the magnetic field line trajectories, it has some constraints, being the most important of them the total neglect of toroidal effects, which are important in many tokamaks [19].

In order to include toroidal corrections, Viana and Caldas proposed a different model for a mapping of the magnetic field lines in a tokamak under influence of ergodic magnetic limiter coils [15]. It consists again of two consecutive mappings : one describing the evolution of the equilibrium field lines, and the other the influence of the perturbation introduced by the ergodic magnetic limiter coils. In this case the perturbative field is considered as being modulated by a delta-peak in the toroidal direction. This approximation may seem rather crude but comparisons with numerical integration

over step-function models have shown that it leads to very good results [8].

The mapping describing the equilibrium field line evolution along the camera is given by:

$$r_n^* = r_n \tag{2.3.a}$$

$$\theta_n^* = \theta_n + \frac{2\pi B_\theta(r_n) R_0}{r_n B_0} \tag{2.3.b}$$

in the cilindrical case, and introducing an usual approximation of the toroidal field correction:

$$B_\phi = \frac{B_0}{1 - \frac{r}{R_0}\cos\theta} \tag{2.4}$$

we obtain the new angular equation with toroidal corrections:

$$\theta_n^* = 2\arctan(\lambda(r_n)\tan(\Omega(r_n) + \arctan\Xi(r_n, \theta_n))) + 2\pi \tag{2.5}$$

where R_0 is the major tokamak radius and $B_\theta(r)$ is the poloidal magnetic field profile, which is related to the safety factor by $B_\theta(r) = \frac{B_0 r}{R_0 q(r)}$. In order to describe the toroidal effects in (2.5) there were also defined some dimensionless variables:

$$\epsilon(r_n) \equiv \frac{r}{R_0} \tag{2.6.a}$$

$$\lambda(r_n) \equiv \frac{1 - \epsilon(r_n)}{\sqrt{1 - \epsilon^2(r_n)}} \tag{2.6.b}$$

$$\Omega(r_n) \equiv \frac{\pi R_0 B_\theta(r_n)(1 - \epsilon(r_n))}{B_0 r_n \lambda(r_n)} \tag{2.6.c}$$

$$\Xi(r_n, \theta_n) \equiv \lambda(r_n)\tan(\frac{\theta_n}{2}) \tag{2.6.d}$$

The impulsive action of the ergodic magnetic limiter on the field lines is described by the mapping:

$$r_{n+1} = r_n^* - bC(\frac{r_n^*}{b})^{m-1}\sin(m\theta_n^*) \tag{2.7.a}$$

$$\theta_{n+1} = \theta_n^* - C(\frac{r_n^*}{b})^{m-2}\cos(m\theta_n^*) \tag{2.7.b}$$

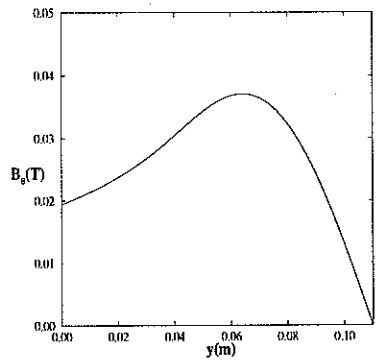

Figure 3: Radial profile of the poloidal field B_θ with TBR-1 parameters.

where we define the dimensionless constant $C \equiv \frac{\mu_0 m I l}{B_0 \pi b^2}$. Plotting Poincaré sections of this mapping, using the TBR-1 parameters (the main parameters are: $R_0 = 0.30m$(major radius), $b = 0.11m$(minor radius), $a = 0.08m$(plasma radius), $B_0 = 0.50T$(toroidal field at magnetic axis), $q(a) = 5$ (safety factor at plasma edge) and $q(0) = 1$ (safety factor at plasma core))[20], and using a well-known empirical model for the radial profile of the poloidal magnetic field:

$$B_\theta(r) = \begin{cases} \frac{aB_\theta(a)}{r}(1 - (1 - \frac{r^2}{a^2})^{\gamma+1}) & (0 < r < a) \\ \frac{aB_\theta(a)}{r} & (a < r < b) \end{cases} \tag{2.8}$$

(fig.3) we observe that for low limiter currents (fig.4a) the island chains and the general structure of the Poincaré plot are well described. But as we increase the limiter current (fig.4b) the small dissipative effects become more important and although there are large regions of irregular field lines, for small values of y, these are not chaotic but are attracted to some island chain by the dissipative effects sooner or later. This also results in more magnetic island destruction than expected, and so this model, although adequated for the study of magnetic island chains at low limiter currents, can not be used for the study at higher currents and the dynamical analisys of chaotic field lines.

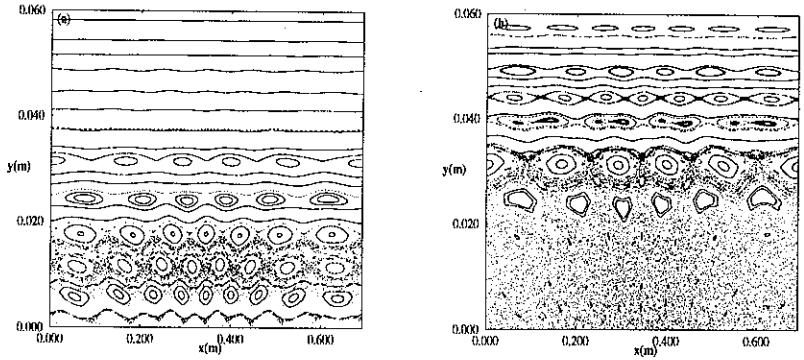

Figure 4: Poincaré sections of the Viana-Caldas mapping with $m = 6$ and (a)$I = 200A$, (b)$I = 800A$ in rectangular coordinates ($x = b\theta$,$y = b - r$).

3 The sympletic model

In order to perform a more accurate study of the onset of chaotic field lines at the tokamak border, we need to develop a field line mapping which can be related directly to the parameters of a given tokamak and is still sympletic [21]. As in the previous models, we split our mapping for the Poincaré section immediately following the ergodic limiter perturbation in two consecutive ones: the first describing the equilibrium field line trajectory along the tokamak camera ($T^1 : (r_n, \theta_n) \to (r_n^*, \theta_n^*)$) and the second describing the effects of the current coils of the ergodic limiter ($T^2 : (r_n^*, \theta_n^*) \to (r_{n+1}, \theta_{n+1})$).

In the cilindrical approximation the equilibrium part of the Viana-Caldas mapping is already sympletic and so we retain it without changes. But we need to introduce a mapping with toroidal corrections that obeys the following conditions:

(a) in the limit $\epsilon = \frac{r}{R_0} \to 0$ it is reduced to the cilindrical mapping;

(b) the new safety factor profile $q(r)$ must be as similar as possible to the profile of the Viana-Caldas mapping, which describes very well the position of the magnetic island chains and their width at low limiter currents;

(c) it must be obtainable from a generating function, which guarantees its sympleticity [21].

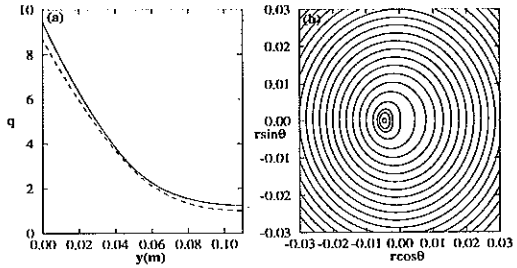

Figure 5: (a) Safety factor profiles for the Viana-Caldas mapping (solid line) and the sympletic mapping (dashed line); (b) Poincaré plot of the sympletic equilibrium mapping with toroidal corrections.

The most generic generating function which insures the properties (a) and (c) above is given by:

$$G^1(\epsilon_n^*, \theta_n) = \theta_n \epsilon_n^* + 2\pi J(\epsilon_n^*) + \sum_{l=1}^{\infty} a_l \epsilon_n^{*l} \cos^l \theta_n \tag{3.1}$$

where we define the normalized radial coordinate $\epsilon \equiv \frac{r}{R_0}$ and the integral of the inverse safety factor $J(\epsilon) = \int_0^{\epsilon} \frac{dx}{q(x)}$. The next step is to fit the arbitrary constants a_l in order to fulfill condition (b). As a matter of fact we verified that a very good profile agreement can be obtained retaining only the first term of the sum with $a_1 = -0.04$ (fig.5a). Using the definiton of this generating function ($\epsilon_n \equiv \frac{\partial G^1}{\partial \theta_n}$ and $\theta_n^* \equiv \frac{\partial G^1}{\partial \epsilon_n^*}$) we obtain the equilibrium mapping equations:

$$r_n^* = \frac{r_n}{1 - a_1 \sin\theta_n} \tag{3.2}$$

$$\theta_n^* = \theta_n + \frac{2\pi}{q(r_n^*)} + a_1 \cos\theta_n \tag{3.3}$$

Plotting the equilibrium curves obtained by this new equilibrium mapping

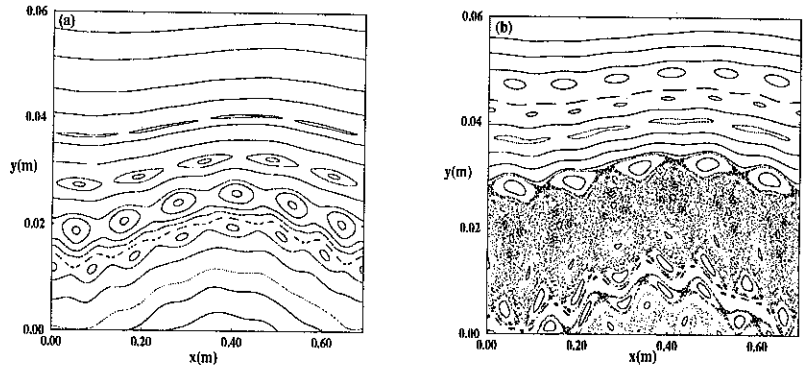

Figure 6: Poincaré sections of the sympletic mapping with $m = 6$ and (a)$I = 200A$, (b)$I = 800A$ in rectangular coordinates.

near the center of the tokamak vessel (fig.5b), we observe that the magnetic axis and the geometric axis are no longer coincident, as in the Viana-Caldas mapping, but there is a displacement between them. This displacement is known in the literature as the Shafranov shift [19, 22] and is well known from numerical solutions of the Grad-Shafranov equation.

In order to obtain a sympletic mapping for the action of the ergodic limiter coils, we retain the angular part:

$$\theta_{n+1} = \theta_n^* - C(\frac{r_n^*}{b})^{m-2}\cos(m\theta_n^*) \tag{3.4}$$

where we use again the adimensional constant $C \equiv \frac{\mu_0 m I \psi}{\pi b^2 B_0}$, and using $\theta_{n+1} \equiv \frac{\partial G^2}{\partial r_{n+1}}$ we obtain the generating function:

$$G^2(r_{n+1}, \theta_n^*) = r_{n+1}\theta_n^* - \frac{Cb}{m-1}(\frac{r_{n+1}}{b})^{m-1}\cos(m\theta_n^*) \tag{3.5}$$

which leads us to the new radial equation given by:

$$r_n^* \equiv \frac{\partial G^2}{\partial \theta_n^*} = r_{n+1} + \frac{mCb}{m-1}(\frac{r_{n+1}}{b})^{m-1}\sin(m\theta_n^*) \tag{3.6}$$

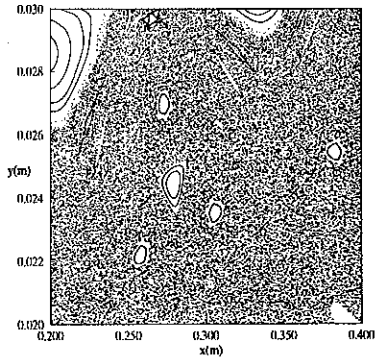

Figure 7: Magnification of detail from the Poincaré plot of fig. 6.b.

Plotting a Poincaré section with this sympletic mapping at low limiter current ($I = 200A$) and using the TBR-1 parameters (fig.6a) we can see that the magnetic island chains at the tokamak camera edge remain very similar to the ones observed in the dissipative Viana-Caldas model (fig.4a) both in their radial position and in their island width. They are only more curved due to the effects of the more realistic toroidal corrections. But as we increase the limiter current to $I = 800A$ the differences between the Poincaré plots are relevant: while in the Viana-Caldas model the structure is destroyed by the small dissipative effects, and so no further dynamical analisys is possible (fig.4b), in the sympletic mapping the island structure with all its details and the onset of global chaos can be observed very precisely (fig.6b), and magnifications of small regions show the typical structure of generic Hamiltonian systems (fig.7).

4 The dynamical analisys of the field lines

One of the most important methods of analisys of non-linear systems is the calculation of Lyapunov exponents, which are defined as [13]:

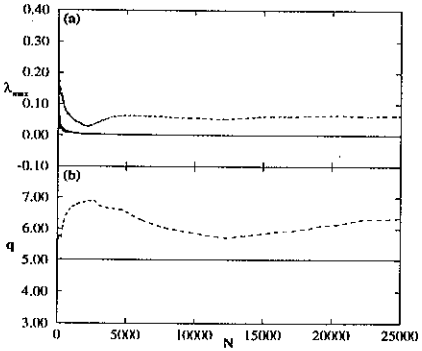

Figure 8: Convergence curves of the (a) Lyapunov exponents and (b) safety factors of a regular trajectory with $x_0 = 0.20m$ and $y_0 = 0.03m$ (solid lines) and a chaotic trajectory with $x_0 = 0.20m$ and $y_0 = 0.02m$ (dashed lines) for the sympletic mapping with $m = 6$ pairs of limiter current coils and $I = 800A$.

$$\lambda_j \equiv \lim_{k\to\infty} \frac{1}{k} \ln \|a_j(\prod_{i=0}^{k} J^i)\| \tag{4.1}$$

where $J^i \equiv \frac{\partial(r_{i+1},\theta_{i+1})}{\partial(r_i,\theta_i)}$ is the Jacobian of the i-th iteration of the mapping and $a_j(M)$ the j-th eigenvalue of a matrix M. For a sympletic mapping it is known that $\sum_i \lambda_i = 0$ and thus for a bidimensional sympletic mapping $\lambda_1 = -\lambda_2$. So we have two possible cases : if $\lambda_1 = \lambda_2 = 0$ for a given trajectory of the system then this trajectory is regular; but, if $\|\lambda_1\| > 0$ then there is exponential divergence of nearby trajectories during the evolution and the trajectory is called chaotic. Of course we can not perform exactly the infinite sum in (4.1) for numerical calculations, but the convergence of the maximum Lyapunov exponent occurs with good precision after just a few thousand iterations, both for regular and chaotic field lines (fig.8a).

Another analisys tool for systems with an angular coordinate is the safety factor, defined for a given trajectory as [23]:

$$q \equiv \lim_{k\to\infty} \frac{2\pi k}{\sum_{j=0}^{k}(\theta_{j+1} - \theta_j)} \tag{4.2}$$

which describes the medium inverse angular shift at each iteration, normalized by a factor 2π. The trajectory can be classified in one of three categories, according to the value of q: if q converges to an irrational number the trajetory is a regular closed torus along the angular coordinate; if q converges to a rational number then the trajectory is either a resonant torus (at $I = 0$) or belongs to a magnetic island chain (for $I > 0$); finally, if q doesn't converge to a real number, the trajectory is chaotic. In fig.8b we can see that for the regular trajectory q converges very quickly (as a matter of fact, we obtain $q = 5$, as the regular trajectory chosen is on the 5/1 magnetic island chain), but for the chaotic trajectory q doesn't converge at all.

With the aid of this two coefficients (the Lyapunov exponent and the safety factor) we are able to characterize completely the dynamical behaviour of a given trajectory, and so we can analyze the relevant phenomena of the transition to chaos, such as island growth and overlapping, and island destruction, as we vary the initial conditions and parameters of our system.

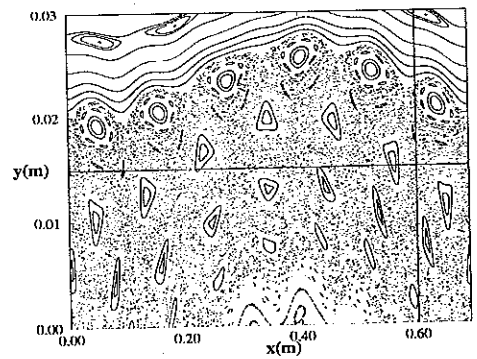

Figure 9: Poincaré section of the sympletic mapping with $m = 7$ and $I = 400A$.

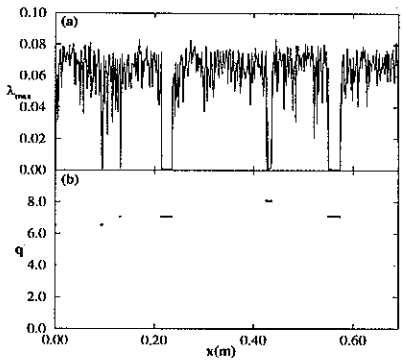

Figure 10: (a) Lyapunov exponents and (b) safety factors along the horizontal line in fig. 9

5 Varying initial conditions and parameters

One of the most used methods in studying the dynamical behaviour of non-linear systems is the plotting of characteristic coefficients (such as the Lyapunov exponents or the safety factors) for varying values of initial conditions or control parameters [1, 2, 24, 25]. If we want to perform a more detailed analisys of a Poincaré section of the sympletic mapping for an intermediate current value (fig.9), where we have chaotic regions, magnetic islands, and a region of undestroyed magnetic tori, one of the possibilities is to calculate the Lyapunov exponents and the safety factors along a horizontal line across the Poincaré section, fixing the initial radial position y_0 (fig.10). We observe that the Lyapunov exponents of the chaotic regions have approximate medium value of $< \lambda > \simeq 0.06$, and the transition from the null exponents in the island regions to the chaotic exponents is quite sudden, i.e., there are no less chaotic transition regions around the islands. Along this section we can observe the crossing of five magnetic islands, in whose interior the safety factors converge: three islands of the $\frac{7}{1}$ chain ($q = 7.0$), one of the $\frac{8}{1}$ chain ($q = 8.0$) and one of the $\frac{13}{2}$ chain ($q = 6.5$); this last island is so small that it can not be seen clearly in the Poincaré section (fig.9) but is clearly detected by the null Lyapunov exponents and the converging safety factors.

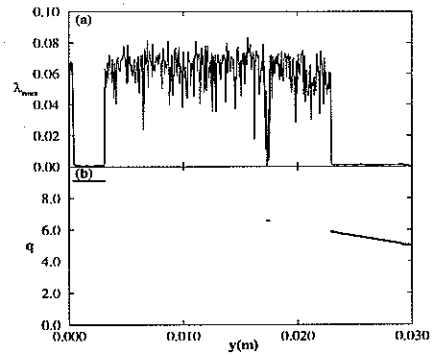

Figure 11: (a) Lyapunov exponents and (b) safety factors along the vertical line in fig. 9

Another possibillity is to analyze a vertical section of the Poincaré plot of fig.9, fixing the initial angular position x_0 (fig.11). In this case we can observe again that $< \lambda > \simeq 0.06$ for all chaotic regions, which means that even the chaotic regions close to the undestroyed tori are no less chaotic than the outer chaotic regions. As for the safety factors, they converge in three distinct regions: there is a large plateau with $q = 9.0$, corresponding to the crossing of the $\frac{9}{1}$ island chain, a very small region with $q = 6.5$, corresponding to the $\frac{13}{2}$ island chain again, and finally there is the region of the undestroyed magnetic field line tori where the safety factors assume the irrational values of each tori, which decrease as we increase y_0. As a matter of fact there are still very small regions of non-convergence of the safety factors in this structure, corresponding to the tiny chaotic layers around the separatrixes of the island chains which are beginning to grow of the resonant tori, but they can be observed only performing large magnifications.

An interesting way to analyse the growing of the magnetic island chains and the onset of chaos, as we increase the limiter current, is to plot the value of the maximum Lyapunov exponent for varying values of the initial radial position y_0 and the limiter current I for a fixed angular position x_0 (fig.12). In this kind of plot we can observe the appearance of the first thin chaotic layers at about $I \simeq 100A$, which grow and join with others to form quite large

chaotic regions as we increase the limiter current. Although this increase of chaotic field lines is very large at first, for higher currents ($I \simeq 500A$) this growing stops because the growing of the inner magnetic surfaces of the island chains and the destruction of the outer ones counterbalance each other. So we can see that analytical predicitions for the growing width of magnetic island chains, such as the square-root rule [8] are valid only for very low currents.

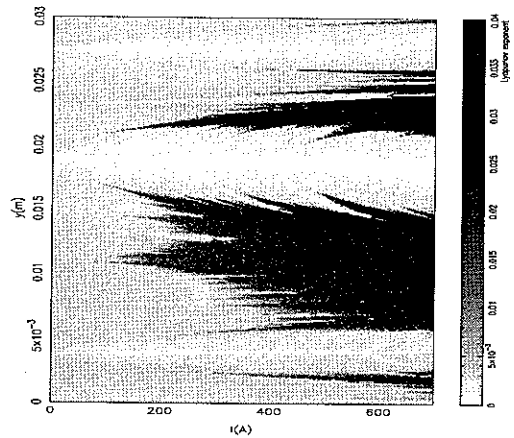

Figure 12: Lyapunov exponents with $m = 6$ and $x_0 = 0.05m$.

If we enlarge a part of this kind of plot (fig.13) we can see that the structure of the frontier between chaotic and regular regions is quite irregular. There are light gray "tongues" entering the borders of the dark chaotic regions, corresponding to secondary island chains which move as we increase the limiter current and are finally destroyed by the growing chaotic region. As each magnetic island has smaller secondary islands, and these islands have other even smaller secondary islands themselves, and so on, the border between the regular and chaotic regions is indeed fractal.

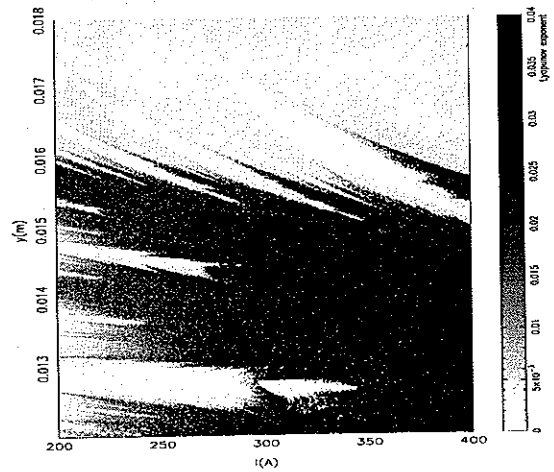

Figure 13: Magnification of detail of fig.12.

6 Conclusions

In this work we introduced a sympletic bidimensional mapping in order to describe the Poincaré section of the magnetic field lines in a tokamak camera under the action of an ergodic limiter. We showed that the sympleticity of the mapping is very important in order to study the behaviour of the chaotic regions at the plasma edge, at high limiter currents. Safety factors and Lyapunov exponents were calculated and the structure of the parameter plane showed very clearly the process of growing and destruction of secondary magnetic islands. It also revealed that at higher limiter currents the chaotic region at the plasma border doesn't grow very much, but remains, approximately, at the same size.

Acknowledgements - The authors would like to thank Dr. C. Ferro-Fontan (Universidad de Buenos Aires, Argentina) for the useful discussions. This work was partially suported by FAPESP and CNPq (Brazilian Government Agencies).

†Electronic address: kai@if.usp.br
‡Electronic address: ibere@if.usp.br

References

[1] M.S. Baptista, I.L. Caldas, Dynamics of the Kicked Logistic Map, *Chaos, Solitons & Fractals* **7**, 325(1996).

[2] K. Ullmann, I.L. Caldas, Transitions in the Parameter Space of a Periodically Forced Dissipative System, *Chaos, Solitons & Fractals*, accepted for publication (1996).

[3] E. Ott, *"Dynamical systems"*, Cambridge University Press (1993).

[4] T. Kapitaniak(Editor) *"Chaotic oscillators"*, World Scientific, Singapore(1991).

[5] N.W. Murray, M.A. Lieberman, A.J. Lichtenberg, Corrections to Quasilinear Diffusion in Area-preserving Maps, *Phys.Rev.* **A32**, 2413(1985).

[6] D. del-Castillo-Negrete, J.M. Greene, P.J. Morrison, Area Preserving Nontwist Maps: Periodic Orbits and Transition to Chaos, *Physica* **D91**, 1(1996).

[7] A. Punjabi, A. Verma, Tokamak Divertor Maps, *J. Plasma Phys.* **52**, 91(1994).

[8] I.L. Caldas, J.M. Pereira, K. Ullmann, R.L. Viana, Magnetic Field Line Mappings for a Tokamak with Ergodic Limiters, *Chaos, Solitons & Fractals* **7**, 991(1996).

[9] A. Punjabi, A. Verma, A. Boozer, Stochastic Broadening of the Separatrix of a Tokamak Divertor, *Phys.Rev.Lett.* **69**, 3322(1992).

[10] F. Karger, K. Lackner, Resonant Helical Divertor, *Phys. Lett.* **A61**, 385(1977).

[11] S. McCool et al., Electron Thermal Confinement Studies with Applied Resonant Fields on TEXT, *Nuclear Fusion* **29**, 547(1989).

[12] S. Habib, R.D. Ryne, Sympletic Calculation of Lyapunov Exponents, *Phys.Rev.Lett.* **74**, 70(1995).

[13] H.G. Schuster, *"Deterministic Chaos"*, Physik Verlag (1984).

[14] T.J.Martin, J.B. Taylor, Ergodic Behaviour in a Magnetic Limiter, *Plasma Phys. and Contr. Fus.* **26**, 321(1984).

[15] R.L. Viana, I.L. Caldas, Peripheral Stochasticity in Tokamaks - The Martin-Taylor Model Revisited, *Zeitschrift für Naturforschung* **47**, 941(1992).

[16] N. Regianni, P.H. Sakanaka, The Effect of the Magnetic Limiter Current on the Peripheral Chaotic Region of a Tokamak, *Plasma Phys. Control. Fusion* **36**, 513(1994).

[17] J.R. Cary, R.G. Littlejohn, Noncanonical Hamiltonian Mechanics and its Application to Magnetic Field Line Flow, *Annals of Physics* **151**, 1(1983).

[18] A.L. Lichtemberg, M.A. Lieberman, *"Regular and Stochastic Motion"*, Springer Verlag, N.Y. (1983).

[19] M.Y. Kucinski, I.L. Caldas, L.H.A. Monteiro, V. Okano, Toroidal Plasma Equilibrium with Arbitrary Current Distribution, *J. Plasma Phys.* **44**, 303(1990).

[20] I.C. Nascimento, I.L. Caldas, R.M.O. Galvão, Tokamak Research at University of São Paulo, *Journal of Fusion Energy* **12**, 529(1994).

[21] A.M.O. de Almeida, On the Sympletically Invariant Variational Principle and Generating Functions, *Proc.R.Soc.Lond.* **A431**, 403(1990).

[22] H.D. Hazeltine, J.D. Meiss, *"Plasma Confinement"*, Addison Wesley, N.Y.(1992).

[23] B. Carreras, H.R. Hicks, B.V. Waddell, Tearing-Mode Activity for Hollow Current Profiles, *Nucl. Fus.* **19**, 583(1979).

[24] J. Rössler, M. Kiwi, B. Hess, M. Markus, Modulated Nonlinear Processes and a Novel Mechanism to Induce Chaos, *Phys. Rev.* **A39**, 5954(1989).

[25] J.A.C. Gallas, Structure of the Parameter Space of the Hénon Map, *Phys.Rev.Lett.* **70**,2714(1993).